A Journal of the Gesellschaft Deutscher Chemiker
Angewandte Chemie
GDCh
International Edition
www.angewandte.org

Accepted Article

Title: Axial TADF Enantiomers Designed for Efficient Blue Circularly Polarized Electroluminescence

Authors: Chuan-Feng Chen, Meng Li, Yin-Feng Wang, Dongdong Zhang, and Lian Duan

To be cited as: *Angew. Chem. Int. Ed.* 10.1002/anie.201914249
Angew. Chem. 10.1002/ange.201914249

Link to VoR: http://dx.doi.org/10.1002/anie.201914249
http://dx.doi.org/10.1002/ange.201914249

WILEY-VCH

COMMUNICATION

Axial TADF Enantiomers Designed for Efficient Blue Circularly Polarized Electroluminescence

Meng Li,* Yin-Feng Wang, Dongdong Zhang, Lian Duan and Chuan-Feng Chen*

Dedication ((optional))

Abstract: A chiral emitting skeleton strategy for the axial TADF enantiomers with CPEL properties has been proposed. Consequently, a pair of chiral stable enantiomers (-)-(*S*)-**Cz-*Ax*-CN** and (+)-(*R*)-**Cz-*Ax*-CN** were designed and synthesized. The enantiomers with both intramolecular π-conjugated charge transfer (CT) and spatial CT not only showed TADF activities with small ΔE_{ST} of 0.029 eV, but also exhibited mirror-image CPL activities with large g_{lum}. Notably, the CP-OLEDs based on the enantiomers emitted blue electroluminescence centered at 468 nm with EQE of 12.5 and 12.7%, and also showed intense CPEL with g_{EL} values of -1.2×10^{-2} and $+1.4\times10^{-2}$, respectively. This is the first CP-OLEDs based on TADF enantiomers with efficient blue CPEL.

Circularly polarized luminescence (CPL) materials, enabling to emit left and right circularly polarized light directly, have aroused considerable attention for their extensive applications in optical quantum information and data storage, chirality sensing, as well as liquid crystal and 3D displays.[1] Although chiral luminophores with circularly polarized photoluminescence (CPPL) have made considerable progress so far,[2] the development of circularly polarized electroluminescence (CPEL) emitters which would be more practical for future display and photonic technologies still lagged behind.[3] Compared with chiral liquid crystal being suffered from temperature-dependent and low efficiencies,[4] circularly polarized organic light-emitting diodes (CP-OLEDs) could be a more prospective strategy to directly emit CPEL for high device performances and simple device architectures. Therefore, since the first CP-OLED was reported in 1997,[5] various CPL materials have been designed for fabricating the CP-OLEDs, including conjugated polymers decorated with chiral sidechains or co-doped with chiral emitters,[6] chiral metal complexes,[7] as well as chiral organic molecules.[8] However, these CPL materials generally displayed unsatisfactory device performances with low external quantum efficiencies (EQEs), which could greatly limit their practical applications.

Recently, thermally activated delayed fluorescence (TADF) materials,[9] as a new generation of high-performance OLED emitters, had successfully been used to design high-efficiency CPL emitters[10] so as to achieve CP-OLEDs with high EQE and intense CPEL.[11] However, the reported CPL materials with TADF activities were almost designed based on the chiral perturbation strategy[10b] (Figure 1a), in which the CPL activities of achiral TADF emitters were mainly induced by using a nonluminous chiral unit. Although this strategy could facilitate the construction of CPL materials with high efficiencies,[11d] the dissymmetry factor (g_{lum} or g_{EL}) values of the materials were generally small probably due to the relatively far of the chiral unit on the CPL materials from their emission unit, and the subsequent uneffective transmission of the chirality to the luminescent unit. Moreover, still no chiral TADF materials with efficient blue CPEL property were reported so far. Therefore, developing new strategies for designing chiral TADF materials and subsequently constructing CP-OLEDs with both high EQEs and large g_{EL} values will be one of most urgent and important topics of this research area.

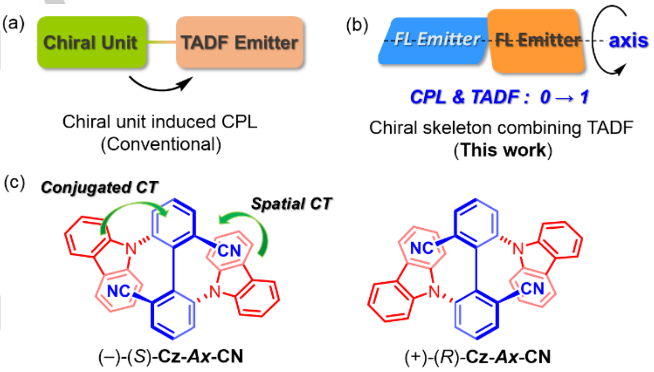

Figure 1. (a) Chiral perturbation strategy, and (b) chiral emitting skeleton strategy. (c) Chemical structures of axial TADF enantiomers.

Herein, we report a chiral emitting skeleton strategy for constructing chiral stable TADF materials with CPEL properties from two fluorophores with no chirality and no TADF property (Figure 1b). Consequently, a pair of axial TADF enantiomers (-)-(*S*)-**Cz-*Ax*-CN** and (+)-(*R*)-**Cz-*Ax*-CN** (Figure 1c) were designed and synthesized by coupling two fluorophores 3-(9H-carbazol-9-yl)benzonitrile (**Cz-CN**). Since the symmetry axis of the designed enantiomers was flanked by different sterically hindered groups, the emitters could form an axial chirality with large racemic energy barriers, which were beneficial to obtain large g_{lum}. Moreover, the enantiomers with intramolecular π-conjugated charge transfer (CT) and spatial CT also exhibited blue TADF activities with small ΔE_{ST} of 0.029 eV. Notably, the CP-OLEDs based on the axial enantiomers not only displayed intense blue electroluminescence (EL) centered at 468 nm with EQE_{max} of up to 12.5 and 12.7%, but also showed CPEL properties with g_{EL} values of -1.2×10^{-2} and $+1.4 \times 10^{-2}$, respectively. This represents the first CP-OLEDs based on TADF enantiomers displaying efficient blue CPEL.

---

[a] Dr. M. Li, Y.-F. Wang, Prof. Dr. C.-F. Chen
CAS Key Laboratory of Molecular Recognition and Function
Institute of Chemistry, Chinese Academy of Sciences
Beijing 100190, China
and
University of Chinese Academy of Sciences, Beijing 100049, China.
E-mail: limeng@iccas.ac.cn, cchen@iccas.ac.cn
[b] Dr. D. Zhang, Prof. Dr. L. Duan
Department of Chemistry, Tsinghua University
Beijing 100084, China

Supporting information for this article is given via a link at the end of the document.

10.1002/anie.201914249

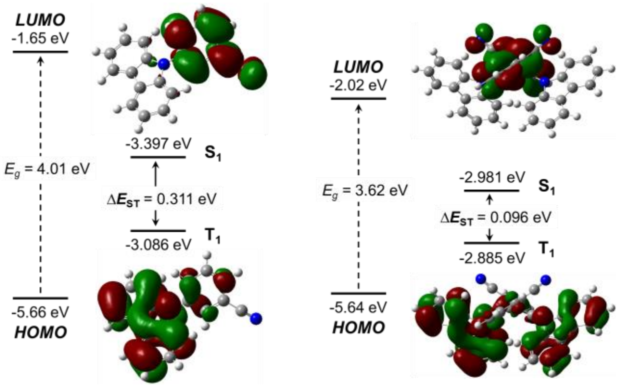

Figure 2. HOMO and LUMO orbital distributions and calculated S_1, T_1 energy levels for **Cz-CN** and **Cz-*Ax*-CN**.

Our design was guided by time-dependent density functional theory calculations, which provided the HOMO-LUMO electronic distribution and the ΔE_{ST} of designed axial enantiomers. As shown in Figure 2, for **Cz-CN** as well as **Cz-*Ax*-CN**, although the HOMO was mainly dispersed on the carbazole unit and the LUMO was localized on the CN-modified phenyl ring, their ΔE_{ST} values were significantly different, which was 0.311 eV for **Cz-CN** and 0.096 eV for **Cz-*Ax*-CN**, respectively (see SI). The calculation results showed that the designed axial enantiomers had TADF properties. Moreover, the electronic distribution covered the entire axial skeleton of the TADF enantiomers, which could ensure the axial enantiomers to have excellent CD and CPL activities.

The designed axial TADF enantiomers (-)-(*S*)-**Cz-*Ax*-CN** and (+)-(*R*)-**Cz-*Ax*-CN** (ee > 99%) were conveniently obtained on gram scale by the copper catalyzed halogenated benzonitrile coupling, and a subsequent substitution reaction with carbazole (Scheme S1), following with optical resolution of racemate *rac*-**Cz-*Ax*-CN** by chiral HPLC. In addition, the specific rotation ($[\alpha]_D^{25}$) of *S*- and *R*-configurations of the axial enantiomers were measured to be –36° and +32° (c = 1.0 mg mL^{-1}, CH_2Cl_2), respectively. The final products were fully characterized by ^{1}H NMR, ^{13}C NMR, high resolution mass spectroscopy, HPLC, and single crystal structure analyses (see SI for details).

With the axial enantiomers in hand, cyclic voltammetry was firstly performed to investigate their electrochemical properties (Figure S17). On the basis of the oxidation curve, the electrochemical HOMO level was estimated as -5.68 eV for (-)-(*S*)-**Cz-*Ax*-CN**. The optical bandgap (E_g) was determined to be 3.28 eV from the onset of the absorption band in thin film, and the LOMO energy level of (-)-(*S*)-**Cz-*Ax*-CN** was then calculated to be -2.40 eV (Table S11). Then, thermal and configurational stabilities of the axial enantiomers were studied to evaluate their reliability. (-)-(*S*)-**Cz-*Ax*-CN** exhibited excellent thermal stabilities with very high decomposition temperatures (T_d) of 388 °C and a glass-transition temperature (T_g) of 260 °C (see SI). Moreover, the remaining enantiomers in the crucible after the fabrication of OLEDs were also analyzed by chiral HPLC. Benefiting from the large steric hindrance of carbazole and cyanogen group, the rotation of the axial enantiomers was limited, which resulted in a large racemic energy barrier. Thus, no racemization of the axial TADF enantiomers had been detected even after multiple sublimations under vacuum (Figure S5-S8). The excellent thermal and configurational stabilities of the axial enantiomers were necessary for improving the performance of CP-OLEDs.

The single crystals of the axial enantiomers and their racemate were obtained successfully. And the single crystal structures showed that the dual fluorescent cores had an axial skeleton with a dihedral angle of 64°. Although the π-conjugation of the entire axial enantiomer was partially interrupted by the large dihedral angle, the C-H⋯π distance from the carbazole on the one fluorophore to the cyano group on the other one was about 2.66 Å (Figure S11a and S13a), which was short enough to ensure their efficient intramolecular spatial charge transfer.[12] The result further confirmed the superiority of the dual fluorescent core design strategy for axial blue TADF emitters.[13] In addition, the absolute configurations of those enantiomers were confirmed by corresponding crystal structures (see Figure 3 and SI for details).

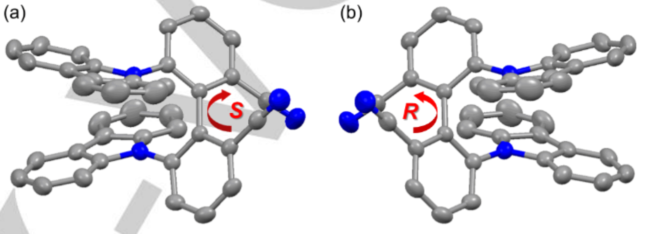

Figure 3. Crystal structures of (a) (-)-(*S*)-**Cz-*Ax*-CN** and (b) (+)-(*R*)-**Cz-*Ax*-CN**.

The photophysical properties of the enantiomers were then investigated. Firstly, the absorption and emission spectra of (-)-(*S*)-**Cz-*Ax*-CN**, being chosen as example, were studied in various solvents. As shown in Figure S18, a relatively weak intramolecular charge transfer absorption band of (-)-(*S*)-**Cz-*Ax*-CN** at about 334 nm was recorded, which was not solvent-dependent in solvents with different polarities. However, with the increase of the solvent polarity, the emission spectra of (-)-(*S*)-**Cz-*Ax*-CN** showed a remarkable redshift from 438 (in hexane) to 502 nm (in methanol), as well as the obvious changes of Stokes shifts and PLQYs (from 14.6 % to 34.7 %, see SI for details). These results indicated the twisted intramolecular charge transfer of the enantiomer in the excited state. Interestingly, when the water fraction (f_w) values of H_2O/THF mixtures was up to 99%, the emission intensities of (-)-(*S*)-**Cz-*Ax*-CN** exhibited significant enhancement (Figure S20), this phenomenon demonstrated that the enantiomers owned aggregation-induced emission (AIE) properties. Furthermore, the photophysical properties of (-)-(*S*)-**Cz-*Ax*-CN** as well as fluorophore **Cz-CN** within pure films were investigated. As shown in Figure S21, owing to the large dihedral angle of axial skeleton, the π-conjugate of the enantiomer was interrupted, thus, the absorption band (λ_{abs} = 335 nm) of the enantiomer was similar to that of **Cz-CN**. However, compared with **Cz-CN** whose emission band and PLQY were 396 nm and 11.9 %, respectively, the emission band of (-)-(*S*)-**Cz-*Ax*-CN** obviously redshift to 473 nm, as well its PLQY significantly elevated to 40.6 % (see Table S13). The results proved once again that our design strategy could significantly improve the PLQY of the obtained enantiomers.

To evaluate the ΔE_{ST} of the axial enantiomers, the emission spectra of (-)-(*S*)-**Cz-*Ax*-CN** (20 wt%) co-doped with bis[2-(diphenylphosphino)phenyl]ether oxide (DPEPO) were investigated at 77 K. The fluorescence and phosphorescence bands of the co-doped film were 460 and 465 nm, respectively,

10.1002/anie.201914249

which resulted in S$_1$ and T$_1$ energy levels of 2.696 and 2.667 eV, respectively (Figure S22). Thus, a small ΔE_{ST} value of 0.029 eV for (-)-(*S*)-**Cz-*Ax*-CN** in the co-doped film was found, which was beneficial to effective reverse intersystem crossing (RISC). In addition, the PLQY of the co-doped film significantly increased to 61.8 %, and when it was measured in vacuum, its PLQY was even up to 68.2 %. Combining with the small ΔE_{ST} and high PLQY, the enantiomers indicated the effective up-conversion of its triplet excitons, thereby achieved excellent TADF activities.

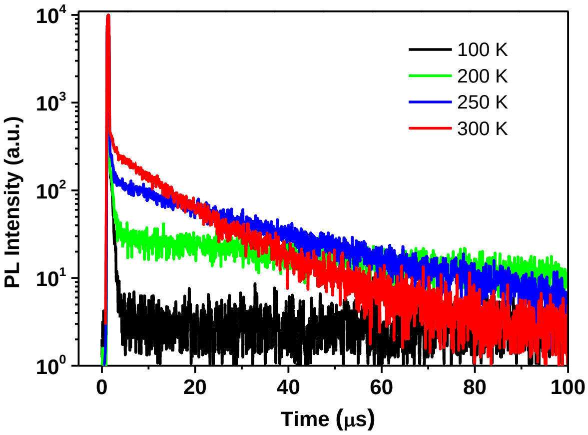

Figure 4. Temperature-dependent transient PL of the co-doped film from 20 wt % (–)-(*S*)-**Cz-*Ax*-CN**:DPEPO.

The transient photoluminescence of (-)-(*S*)-**Cz-*Ax*-CN** was further measured in the co-doped film. As shown in Figure S25a, the transient decay curve of (-)-(*S*)-**Cz-*Ax*-CN** showed two exponential decays at 300 K, which were prompt fluorescence lifetime (τ_{PF}) of 30 ns and delayed conponent (τ_{DF}) of 12.6 μs, respectively. The delayed fluorescence spectra (after 5 μs and 10 μs) of the enantiomers were identical to the emission spectra without a delay (Figure S25b), which indicated that the delayed fluorescence was related to the delayed component by RISC.[14] The short τ_{DF} of the enantiomer could effectively suppress the annihilation of its triplet excitons in the devices, thus being beneficial for low efficiency roll-off. Then, the rates of the various transition processes of (-)-(*S*)-**Cz-*Ax*-CN** were calculated by using its fluorescence lifetime and PLQYs. As shown in Table S15, the singlet state radiative rate (k_r^S) and intersystem crossing rate (k_{ISC}) were 1.18 × 10^7 s^{-1} and 2.15 × 10^7 s^{-1}, respectively, which indicated that the emission of S$_1$ excitons was almost simultaneous with the generation of T$_1$ excitons. Meanwhile, since the RISC of T$_1$ excitons was spin-forbidden, the RISC rate (k_{RISC} = 1.32 × 10^5 s^{-1}) and delayed fluorescence rate (k_{DF} = 7.94 × 10^4 s^{-1}) were relatively slower. In addition, the temperature-dependent transient PL of (-)-(*S*)-**Cz-*Ax*-CN** were studied as well. As shown in Figure 4, the delayed component of the transient PL gradually increased, meanwhile the phosphorescence lifetime disappeared gradually with the temperature from 100 to 300 K. This phenomenon indicated more favorable RISC of excitons from T$_1$ to S$_1$ by gradual warming. The efficient RISC process, as well as the small ΔE_{ST} value and high PLQYs of the enantiomers demonstrated the TADF activities of the designed axial enantiomers, which were also crucial for high performance device.

To further characterize the chiroptical properties of the axial enantiomers, CD and CPL spectra of the enantiomers were investigated. The obvious mirror-image CD spectra of the enantiomers were observed with alternating positive and negative Cotton effects (Figure 5), among which, the intense Cotton effects in short wavelength regions were assigned to absorption producing by the intramolecular π-conjugated CT. Meanwhile, the weak Cotton effects at the maximum absorption band were caused by intramolecular spatial CT. The results indicated that the chirality of the enantiomers in the ground state could be successfully formed by the chiral emitting skeleton strategy. Furthermore, the enantiomers also displayed almost mirror-image CPL spectra with the g_{lum} values of -4.8 × 10^{-3} for (–)-(*S*)-**Cz-*Ax*-CN** and +4.5 × 10^{-3} for (+)-(*R*)-**Cz-*Ax*-CN**, respectively, and the g_{lum} values of which were larger than that of the CPL emitters obtained by traditional chiral perturbation strategy. The results also demonstrated that our chiral emitting skeleton strategy could produce novel chiral emitters, which not only had efficient blue TADF properties, but also possessed CPL activities with large g_{lum}.

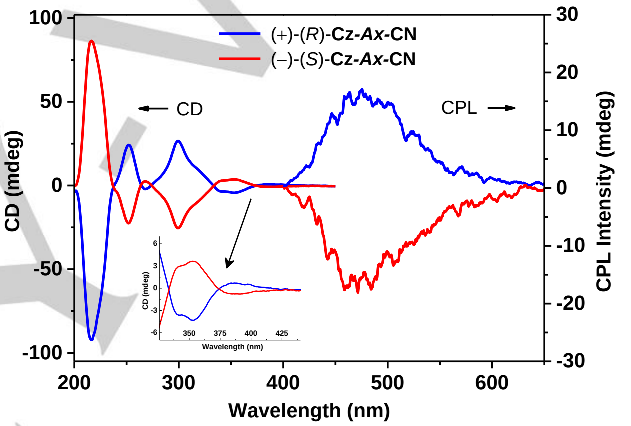

Figure 5. CD and CPL spectra of (–)-(*S*)-**Cz-*Ax*-CN** and (+)-(*R*)-**Cz-*Ax*-CN** in film states.

The enantiomers were then used as emissive dopants to fabricate CP-OLEDs with the following architecture: ITO/HAT-CN /TAPC/mCP/20 wt% (*S*/*R*)-**Cz-*Ax*-CN**:DPEPO/TSPO1/TPBi/LiF /Al (Figure 6a). The EL spectra of the devices based on (–)-(*S*)-**Cz-*Ax*-CN** displayed gratifying blue EL centered at 468 nm (Figure 6b). Moreover, the device also presented a turn-on voltage (V$_T$) of 4.0 V, and high efficiencies with maximum current efficiency (CE$_{max}$), power efficiency (PE$_{max}$) and EQE$_{max}$ of 20.6 cd A^{-1}, 15.4 lm W^{-1}, 12.5 %, respectively. Moreover, the device based on the enantiomer also showed relatively low efficiency roll-off, and the EQE values of which were 11.1 % and 8.8 % at the luminance of 100 and 1000 cd m^{-2}, respectively. Meanwhile, since the photophysical properties of the two enantiomers were almost identical, the EL performances of their devices were also similar. For (+)-(*R*)-**Cz-*Ax*-CN** based device, the performances showed blue EL centered at 468 nm, a V$_T$ of 4.0 V, a CE$_{max}$ of 20.9 cd A^{-1}, a PE$_{max}$ of 16.4 lm W^{-1}, and a EQE$_{max}$ of 12.7 %, respectively. These results indicated that the enantiomers formed by dual fluorescent cores could efficiently realize the construction of TADF emitters, and then obtain high-efficiency blue OLEDs.

Subsequently, the CPEL characteristics of the enantiomer based CP-OLEDs were studied. As illustrated in Figure 6c, the enantiomers based devices resulted in obvious blue CPEL activities with opposing g_{EL} signals. And the g_{EL} values of the CP-

OLEDs were -1.2×10^{-2} for (–)-(*S*)-**Cz-*Ax*-CN** and $+1.4 \times 10^{-2}$ for (+)-(*R*)-**Cz-*Ax*-CN**, respectively, which were larger than the g_{EL} values of most TADF enantiomers based on chiral perturbation strategy. The results further confirmed that by our chiral emitting skeleton strategy based on dual fluorescent cores, chiral TADF materials with both high efficiencies and intense CPEL of large g_{EL} values could be conveniently obtained. This is also the first CP-OLEDs with efficient blue CPEL based on TADF enantiomers.

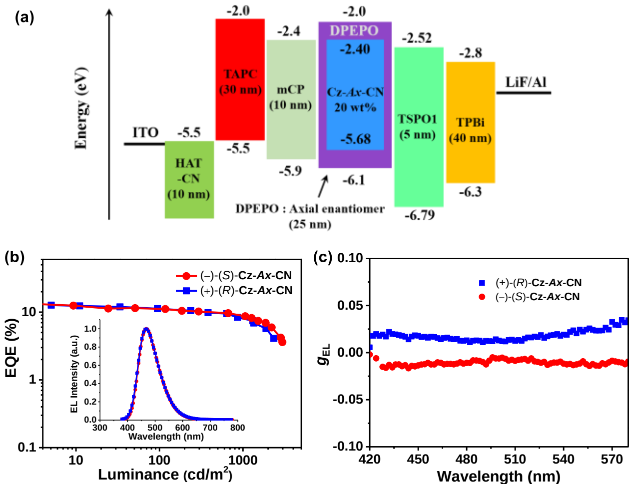

Figure 6. The energy diagram (a) and performance of CP-OLEDs based on (–)-(*S*)-**Cz-*Ax*-CN** and (+)-(*R*)-**Cz-*Ax*-CN**. (b) EQE-luminance characteristics. Inset: EL spectra of the devices at 6 V. (c) The g_{EL} values of the devices as a function of emission wavelength.

In summary, we proposed a chiral emitting skeleton strategy for designing axial TADF enantiomers with CPL activities, and thus fabricating CP-OLEDs with high EQEs and large g_{EL} values. The enantiomers with rigid chiral axis obtained by coupling two fluorophores exhibited both intramolecular π-conjugated CT and spatial CT, which resulted in not only excellent blue TADF properties of small ΔE_{ST} (0.029 eV), high PLQY (68.2%), and short delayed fluorescence lifetime (12.6 μs), but also mirror-image CPL activities with g_{lum} values of -4.8×10^{-3} and $+4.5 \times 10^{-3}$, respectively. Notably, the axial enantiomer-based CP-OLEDs displayed high EQEs of 12.5 and 12.7%, respectively, and intense CPEL with g_{EL} values of -1.2×10^{-2} and $+1.4 \times 10^{-2}$, respectively, which also represented the first CP-OLEDs based on TADF enantiomers with efficient blue CPEL. Our new strategy presented herein provides a promising design for chiral luminescent materials with both high efficiencies and large g_{lum} values, which could greatly promote the development of CP-OLEDs, and even future 3D display application.

Acknowledgements

We thank the National Natural Science Foundation of China (21871272, 91956119, 21521002), and the Youth Innovation Promotion Association CAS (No. 2019034) for financial supports. We also thank Dr. F. Song for collecting the CPEL signals.

Keywords: CP-OLEDs • TADF • axial enantiomer • blue electroluminescence • circularly polarized electroluminescence

[1] a) R. Farshchi, M. Ramsteiner, J. Herfort, A. Tahraoui, H. T. Grahn, *Appl. Phys. Lett.* **2011**, *98*, 162508; b) Y. Yang, R. C. da Costa, M. J. Fuchter, A. J. Campbell, *Nat. Photonics* **2013**, *7*, 634-638; c) D.-Y. Kim, *J. Korean Phys. Soc.* **2006**, *49*, 505-508.

[2] a) Y. Sang, J. Han, T. Zhao, P. Duan, M. Liu, *Adv. Mater.* **2019**, 1900110; b) K. Takaishi, S. Hinoide, T. Matsumoto, T. Ema, *J. Am. Chem. Soc.* **2019**, *141*, 11852-11857; c) J. Zhao, T. Zhang, X.-Y. Dong, M.-E. Sun, C. Zhang, X. Li, Y. S. Zhao, S.-Q. Zang, *J. Am. Chem. Soc.* **2019**, *141*, 15755-15760.

[3] J. Han, S. Guo, H. Lu, S. Liu, Q. Zhao, W. Huang, *Adv. Opt. Mater.* **2018**, *6*, 1800538.

[4] M. Oda, H. G. Nothofer, G. Lieser, U. Scherf, S. C. J. Meskers, D. Neher, *Adv. Mater.* **2000**, *12*, 362-365.

[5] E. Peeters, M. P. T. Christiaans, R. A. J. Janssen, H. F. M. Schoo, H. P. J. M. Dekkers, E. W. Meijer, *J. Am. Chem. Soc.* **1997**, *119*, 9909-9910.

[6] a) Y. Yang, R. C. da Costa, D.-M. Smilgies, A. J. Campbell, M. J. Fuchter, *Adv. Mater.* **2013**, *25*, 2624-2628; b) D.-M. Lee, J.-W. Song, Y.-J. Lee, C.-J. Yu, J.-H. Kim, *Adv. Mater.* **2017**, *29*, 1700907; c) L. Wan, J. Wade, F. Salerno, O. Arteaga, B. Laidlaw, X. Wang, T. Penfold, M. J. Fuchter, A. J. Campbell, *ACS Nano* **2019**, *13*, 8099-8105.

[7] a) F. Zinna, U. Giovanella, L. Di Bari, *Adv. Mater.* **2015**, *27*, 1791-1795; b) J. R. Brandt, X. H. Wang, Y. Yang, A. J. Campbell, M. J. Fuchter, *J. Am. Chem. Soc.* **2016**, *138*, 9743-9746; c) F. Zinna, M. Pasini, F. Galeotti, C. Botta, L. Di Bari, U. Giovanella, *Adv. Funct. Mater.* **2017**, *27*, 1603719; d) J. Han, S. Guo, J. Wang, L. Wei, Y. Zhuang, S. Liu, Q. Zhao, X. Zhang, W. Huang, *Adv. Opt. Mater.* **2017**, *2*, 1700359.

[8] a) M. Li, W.-B. Lin, L. Fang, C.-F. Chen, *Acta Chim. Sinica* **2017**, *75*, 1150-1163; b) X. Zhang, Y. Zhang, Y. Li, Y. Quan, Y. Cheng, Y. Li, *Chem. Commun.* **2019**, *55*, 9845-9848; c) X. Zhang, Y. Zhang, H. Zhang, Y. Quan, Y. Li, Y. Cheng, S. Ye, *Org. Lett.* **2019**, *21*, 439-443.

[9] H. Uoyama, K. Goushi, K. Shizu, H. Nomura, C. Adachi, *Nature* **2012**, *492*, 234-238.

[10] a) T. Imagawa, S. Hirata, K. Totani, T. Watanabe, M. Vacha, *Chem. Commun.* **2015**, *51*, 13268-13271; b) S. Feuillastre, M. Pauton, L. Gao, A. Desmarchelier, A. J. Riives, D. Prim, D. Tondelier, B. Geffroy, G. Muller, G. Clavier, G. Pieters, *J. Am. Chem. Soc.* **2016**, *138*, 3990-3993; c) N. Sharma, E. Spuling, C. M. Mattern, W. Li, O. Fuhr, Y. Tsuchiya, C. Adachi, S. Bräse, I. D. W. Samuel, E. Zysman-Colman, *Chem. Sci.* **2019**, *10*, 6689-6696.

[11] a) M. Li, S.-H. Li, D. Zhang, M. Cai, L. Duan, M.-K. Fung, C.-F. Chen, *Angew. Chem. Int. Ed.* **2018**, *57*, 2889-2893; *Angew. Chem.* **2018**, *130*, 2939-2943; b) F. Song, Z. Xu, Q. Zhang, Z. Zhao, H. Zhang, W. Zhao, Z. Qiu, C. Qi, H. Zhang, H. H. Y. Sung, I. D. Williams, J. W. Y. Lam, Z. Zhao, A. Qin, D. Ma, B. Z. Tang, *Adv. Funct. Mater.* **2018**, *28*, 1800051; c) Z.-G. Wu, H.-B. Han, Z.-P. Yan, X.-F. Luo, Y. Wang, Y.-X. Zheng, J.-L. Zuo, Y. Pan, *Adv. Mater.* **2019**, *31*, 1900524.

[12] H. Tsujimoto, D.-G. Ha, G. Markopoulos, H. S. Chae, M. A. Baldo, T. M. Swager, *J. Am. Chem. Soc.* **2017**, *139*, 4894-4900.

[13] a) Y. J. Cho, S. K. Jeon, B. D. Chin, E. Yu, J. Y. Lee, *Angew. Chem. Int. Ed.* **2015**, *54*, 5201-5204; *Angew. Chem.* **2015**, *127*, 5290-5293; b) Y. J. Cho, S. K. Jeon, S.-S. Lee, E. Yu, J. Y. Lee, *Chem. Mater.* **2016**, *28*, 5400-5405.

[14] M. Li, Y. Liu, R. Duan, X. Wei, Y. Yi, Y. Wang, C.-F. Chen, *Angew. Chem. Int. Ed.* **2017**, *56*, 8818-8822; *Angew. Chem.* **2017**, *129*, 8944-8948.

10.1002/anie.201914249

COMMUNICATION

A chiral emitting skeleton strategy for designing the axial TADF enantiomers with CPEL properties has been proposed. The CP-OLEDs based on the enantiomers displayed high efficiencies and blue CPEL with large g_{EL} values.

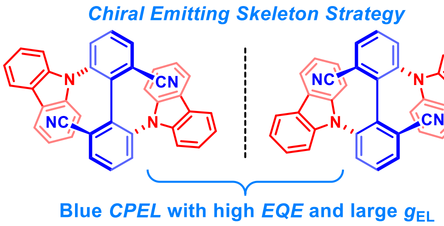

Meng Li, Yin-Feng Wang, Dongdong Zhang, Lian Duan and Chuan-Feng Chen**

Page No. – Page No.

Axial TADF Enantiomers Designed for Efficient Blue Circularly Polarized Electroluminescence